Environmental Research Communications

LETTER

# The surface downward longwave radiation of the CMIP6 HighResMIP in East Asia offline corrected by the three-dimensional sub-grid terrain longwave radiative effect scheme

**Chunlei Gu**[1], **Anning Huang**[1,2], **Xin Li**[3] and **Yang Wu**[3]

[1] School of Atmospheric Sciences, Nanjing University, Nanjing, 210023, People's Republic of China
[2] Qinghai Lake Comprehensive Observation Research station, Chinese Academy of Sciences, Gangcha, 812300, People's Republic of China
[3] Key Laboratory of Transportation Meteorology of China Meteorological Administration, Nanjing Joint Institute for Atmospheric Sciences, Chinese Academy of Meteorological Sciences - Jiangsu Meteorological Service, Nanjing, 210041, People's Republic of China

**E-mail:** anhuang@nju.edu.cn

**Keywords:** surface downward longwave radiation, CMIP6 HighResMIP, East Asia, offline correction, three-dimensional sub-grid terrain longwave radiative effect scheme

OPEN ACCESS

RECEIVED
12 August 2024

REVISED
18 September 2024

ACCEPTED FOR PUBLICATION
1 October 2024

PUBLISHED
24 October 2024



## Abstract

Terrain significantly regulates surface downward longwave radiation (SDLR). The CMIP6 HighResMIP models without the three-dimensional sub-grid terrain longwave radiative effects (3DSTLRE) produce large SDLR biases over complex terrains. This study applies the 3DSTLRE scheme to correct the SDLR simulated by these models in East Asia and assesses the correction's effectiveness. Results indicate that the CMIP6 HighResMIP models without the 3DSTLRE clearly underestimate the SDLR over the rugged terrains and the underestimation increases with the sub-grid terrain complexity. The offline correction of 3DSTLRE can evidently improve the SDLR simulations in different seasons, and the improvements increase with the sub-grid terrain complexity. The most significant improvements are observed over the Himalayas, the Tibetan Plateau, the Tianshan Mountains, and the Hengduan Mountains. The relative root mean square error of SDLR simulations over the areas with the most complex sub-grid terrains can be decreased by ~40% due to the offline correction of 3DSTLRE. Considering the 3DSTLRE may be an efficient way to improve the simulations of the SDLR and surface energy balance over the regions with complex sub-grid terrains.

## 1. Introduction

The surface downward longwave radiation (SDLR) is an important component of the surface energy balance, driving local weather patterns and global climate change (Wang and Liang 2009, Feng *et al* 2023). The SDLR is the primary heat source that warms the land surface under specific conditions, such as low solar elevation, nighttime, deep valleys, high latitudes, and glaciers that are starting to melt (Whiteman *et al* 1989, Matzinger *et al* 2003, Juszak and Pellicciotti 2013, Zhang *et al* 2013, Senese *et al* 2020). The SDLR is sensitive to global warming (Vargas Zeppetello *et al* 2019, Stephens *et al* 2012). Inaccurate simulations of the SDLR in numerical models can increase the uncertainty associated with simulated soil freeze–thaw processes, snow and ice melting, canopy temperature, near-surface temperatures, and subsequent atmospheric circulation (Wu *et al* 2016, Webster *et al* 2017, Lee *et al* 2019, Robledano *et al* 2022, Luo *et al* 2023). Over the plane surface, the SDLR is determined by the radiative effects of the cloud and the atmospheric conditions, such as low-level humidity, greenhouse gases, and air temperature (Sugita and Brutsaert 1993, Viúdez-Mora *et al* 2015, Shakespeare and Roderick 2022, Tana *et al* 2023, Shang *et al* 2024).

Over the mountainous region, the SDLR is not only determined by the atmospheric radiative transfer but also significantly influenced by the topographical relief (Olyphant 1986, Yan *et al* 2020). The topographies can block the SDLR from the sky and emit additional longwave radiation to the neighbouring point (Duguay 1993, Robledano *et al* 2022). The longwave radiative effects of terrain have been studied since the late 1970s

(Cole 1979, Dozier and Outcalt 1979) and widely applied in hydrological simulation and generating the SDLR data based on the Geographic Information System (Gratton *et al* 1993, Arnold *et al* 2006, Yan *et al* 2016, Wu *et al* 2019). The SDLR can be increased by $10^1 \sim 10^2$ $Wm^{-2}$ due to the extra longwave radiation emitted from the surrounding terrains (Aubry-Wake *et al* 2018, Zhu *et al* 2018, Yan *et al* 2020, Feldman *et al* 2022).

Since the 2000s, the significance of sub-grid terrain effects has been acknowledged in numerical models because of the increasing horizontal model resolution (Hauge and Hole 2003, Müller and Scherer 2005, Chen *et al* 2006, Zhang *et al* 2006, Essery and Marks 2007). The sub-grid terrain solar radiative effects have been widely applied in weather/climate numerical models (Feng and Zhang 2007, Liou *et al* 2007, Lai *et al* 2010, Lee *et al* 2011, Ruiz-Arias *et al* 2011, Gu *et al* 2012, Manners *et al* 2012, Arthur *et al* 2018, Fan *et al* 2019, He *et al* 2019, Hao *et al* 2021, Gu *et al* 2022, Huang *et al* 2022, Zhang *et al* 2022, Cai *et al* 2023). However, the sub-grid longwave radiative effects are not well described in numerical models. Some studies have found that incorporating sub-grid longwave radiative effects into regional climate models can enhance the simulation of surface energy balance and, consequently, precipitation (Zhang *et al* 2006, Feng and Zhang, 2007, Gu *et al* 2020). But they only consider the obstruction of SDLR caused by the topography and completely ignore the additional longwave radiation emitted from the topography. Recently, based on the mountain radiation theory, we have developed a three-dimensional sub-grid terrain longwave radiative effects (3DSTLRE) parameterization scheme (Gu *et al* 2024a), which fully accounts for the terrain obstruction of the SDLR from the sky and the additional SDLR emitted from the surrounding terrains.

The High Resolution Model Intercomparison Project (HighResMIP, Haarsma *et al* 2016) is an important component of the World Climate Research Programme (WCRP) Coupled Model Intercomparison Project Phase 6 (CMIP6). The CMIP6 HighResMIP aims to systematically investigate the impact of horizontal resolution. The HighResMIP gathers state-of-the-art global climate models and conducts simulations spanning the period 1950–2050 (Roberts *et al* 2020, Priestley and Catto 2022). However, the CMIP6 HighResMIP models do not consider the three-dimensional sub-grid terrain longwave radiative effects (3DSTLRE), which may result in additional uncertainty of SDLR simulations over the rugged areas compared to the plains (Wan *et al* 2022, Xu *et al* 2022). Recent study of Gu *et al* (2024b) indicated that the biases in the CMIP6 HighResMIP surface solar irradiance simulations offline corrected by the three-dimensional sub-grid terrain solar radiative effects (3DSTSRE) can be significantly reduced over the rugged areas. Besides the 3DSTSRE, the 3DSTLRE is also crucial for accurately describing the surface energy balance.

In this study, the 3DSLTRE scheme provided by Gu *et al* (2024a) is used to offline correct the CMIP6 HighResMIP SDLR simulations. One purpose of this study is to evaluate additional uncertainty of the SDLR simulated by the CMIP6 HighResMIP models without the 3DSTLRE over the mountainous areas relative to the plains. The other purpose is to provide a method for correcting the CMIP6 HighResMIP SDLR simulations. The corrected SDLR simulations may be better utilized in studying the surface energy balance, exploring the physical mechanism of climate change, and as the forcing data for the land surface model, the glacier model, and the hydrological models (Ren *et al* 2018, Tao and Barros 2018, Wild 2020, Heavens 2021, Van Beusekom *et al* 2022, Liu *et al* 2023, Wang *et al* 2023, Shi *et al* 2024, Wu *et al* 2024). The East Asia region was selected as the study area for three reasons. First, East Asia features some of the most complex terrains in the world, including the Himalayas, the Tibetan Plateau, the Hengduan Mountains, and the Tianshan Mountains (figure 1(a)). Second, the climate of East Asia is significantly influenced by these diverse terrains (Huang *et al* 2023). The last point is that East Asia exhibits significant SDLR biases produced by the CMIP6 HighResMIP models (Xu *et al* 2022). The rest of the paper is arranged as follows: The data, methodology, and metrics are introduced in section 2. Section 3 presents the results. The discussion and conclusion are described in section 4.

## 2. Data, methodology and metrics

### 2.1. Data

The data used in this study are listed as follows:

The sub-grid terrain is provided by the Shuttle Radar Topography Mission (SRTM) Version 4.1 (Jarvis et al 2008) digital elevation model (DEM) data with a horizontal resolution of 3″ (~90 m).

The monthly surface upward longwave radiation (SULR) and SDLR fluxes from the 11 CMIP6 HighResMIP models participating the *hist*-1950 experiment during 2001–2014 (specific information shown in table 1).

The SDLR observations during 2001–2014 from the monthly CMSAF Cloud, Albedo and Surface Radiation dataset (CLARA-A2, Karlsson et al 2020) with a horizontal resolution of 0.25°, which takes into account the effects of topography on the SDLR (Karlsson *et al* 2017).

The SDLR observations during 2001–2014 from the monthly Synoptic TOA and surface fluxes and clouds dataset (SYN1deg_Ed4.1) with a horizontal resolution of 1° provided by the Clouds and the Earth's Radiant Energy System (CERES) project (Doelling *et al* 2016). The SDLR from the CERES aligns well with the station

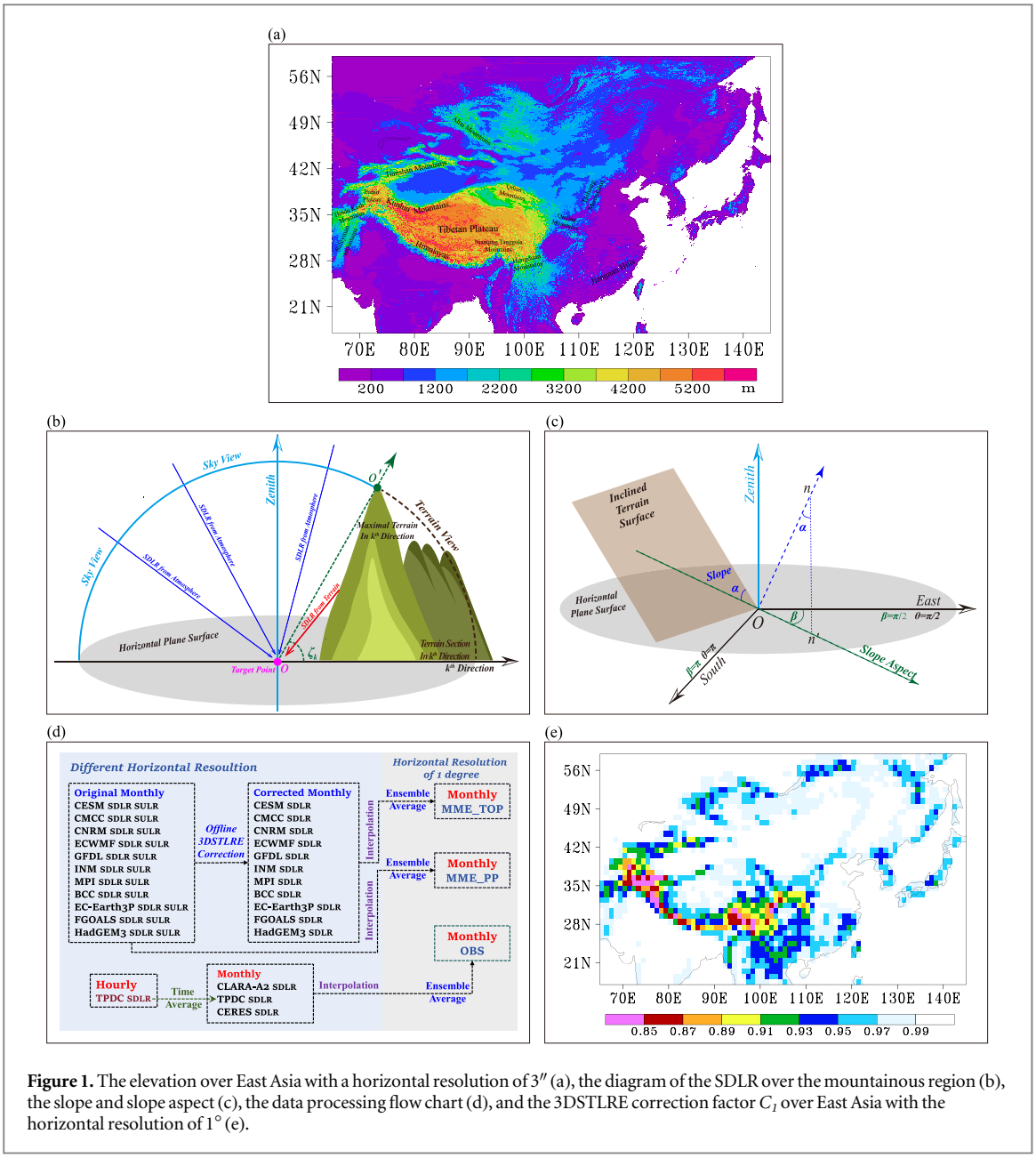


**Figure 1.** The elevation over East Asia with a horizontal resolution of 3″ (a), the diagram of the SDLR over the mountainous region (b), the slope and slope aspect (c), the data processing flow chart (d), and the 3DSTLRE correction factor $C_1$ over East Asia with the horizontal resolution of 1° (e).

observations in the regions with high elevation and complex terrain, such as the Tibetan Plateau and the Loess Plateau (Gui *et al* 2010, Yan *et al* 2011, Naud *et al* 2012, Wang *et al* 2021) and is broadly applied in the studies of the surface energy balance over East Asia (Chen *et al* 2022, Wang *et al* 2022).

The hourly fused global land surface longwave downward radiation dataset with a horizontal resolution of 0.25° during 2001–2014 provided by the National Tibetan Plateau/Third Pole Environment Data Center (TPDC, Wang and Wang 2022, Wang *et al* 2022), which is an enhanced product that combines satellite data and reanalysis data using a machine learning-based fusion method.

The simulated SULR and SDLR fluxes from the CMIP6 HighResMIP models and the SRTM DEM data are used for the offline correction. The SDLR fluxes from the CLARA-A2, the CERES, and the TPDC are used for the evaluation. The simulated SDLR fluxes and the satellite-observed SDLR fluxes are available at monthly or daily intervals, which limits our ability to analyze the diurnal effects of the offline 3DSTLRE correction. Consequently, this study examines the impacts of 3DSTLRE on a monthly and seasonal scale.

### 2.2. The 3DSTSRE scheme

The SDLR fluxes contain two components: namely the SDLR coming from the atmosphere and the SDLR emitted from the surrounding topography (figure 1(b)). The sky view factor (*SVF*) is used to measure the openness of the sky, which is the ratio of the obstructed sky to the total sky (Dirksen *et al* 2019, Jiao *et al* 2019). The *SVF* varies from 0.0 to 1.0, representing the degree to which the sky over the target point is obstructed,

**Table 1.** The models of CMIP6 HighResMIP providing the data in this study.

| Model | Horizontal resolution | Institution | Model description | Data source |
|---|---|---|---|---|
| BCC-CSM2-HR | ~50 km | Beijing Climate Center | Wu *et al* (2021) | Jie *et al* (2020) |
| CESM1-CAM5-SE-HR | ~25 km | National Center for Atmospheric Research, Climate and Global Dynamics Laboratory | Chang *et al* (2020) | Hurrel *et al* (2020) |
| CMCC-CM2-VHR4 | ~25 km | Fondazione Centro Euro-Mediterraneo sui Cambiamenti Climatici | Scoccimarro *et al* (2022) | Scoccimarro *et al* (2018) |
| CNRM-CM6-1-HR | ~50 km | Centre National de Recherches Meteorologiques, Centre Europeen de Recherche et de Formation Avancee en Calcul Scientifique | Saint-Martin *et al* (2021) | Voldoire (2019) |
| EC-Earth3P-HR | ~50 km | EC-Earth-Consortium | Haarsma *et al* (2020) | EC-Earth Consortium (2018) |
| ECMWF-IFS-HR | ~25 km | European Centre for Medium-Range Weather Forecasts | Roberts *et al* (2018) | Roberts *et al* (2017) |
| FGOALS-f3-H | ~25 km | Chinese Academy of Sciences | An *et al* (2022) | Yu (2020) |
| GFDL-CM4C192 | ~50 km | National Oceanic and Atmospheric Administration, Geophysical Fluid Dynamics Laboratory | Zhao *et al* (2018a) | Zhao *et al* (2018b) |
| HadGEM3-GC31-HH | ~50 km | Met Office Hadley Centre | Roberts *et al* (2019) | Roberts (2021) |
| INM-CM5-H | ~50 km | Institute for Numerical Mathematics, Russian Academy of Science | Volodin *et al* (2017) | Volodin *et al* (2019) |
| MPI-ESM1–2-XR | ~50 km | Max Planck Institute for Meteorology | Gutjahr *et al* (2019) | von Storch *et al* (2018) |

ranging from completely obstructed to completely unobstructed. The terrain view factor (1.0-*SVF*) is the counterpart of the sky view factor, representing the ratio of the sky obstructed by the topography. The SDLR over the sub-grid with the rugged surface ($L_{t\downarrow}$) can be calculated by equation (1) (Robledano *et al* 2022):

$$L_{t\downarrow} = SVF{\cdot}L_{p\downarrow} + (1 - SVF){\cdot}L_{sur} \tag{1}$$

Where $L_{p\downarrow}$, $L_{sur}$, $SVF$, and $(1 - SVF)$ are the SDLR over the plane surface, the longwave radiation emitted from the surrounding terrain, the sky view factor, and the terrain view factor. The $SVF$ can be calculated by equation (2) (Dozier and Frew,1990):

$$SVF = \frac{1}{N}\sum_{k=1}^{N}\left[\sin\alpha{\cdot}\cos(\theta_k - \beta)\left(\frac{\pi}{2} - \zeta_k - \sin\zeta_k{\cdot}\cos\zeta_k\right) + \cos\alpha{\cdot}\cos^2\zeta_k\right] \tag{2}$$

Where $\alpha$ and $\beta$ are the terrain slope and aspect of the target point. The $\theta_k$ and $\zeta_K$ are the azimuth and the maximal terrain elevation angle at the $K^{th}$ direction. $N$ is the total number of the divided direction. Larger $N$ leads to more accuracy of $SVF$ but cost more computation. $N$ is set to 360 in this study. As shown in figure 1(c), the $\alpha$ represents the terrain steepness and varies from 0.0 to $\frac{\pi}{2}$. The $\beta$ is the orientation of the slope and varies from 0.0 to $2\pi$. The $\beta$ is 0.0, $\frac{\pi}{2}$, $\pi$, and $\frac{3\pi}{2}$ in the north, east, south, and west direction, respectively. The $\alpha$ and $\beta$ can be calculated by the horizontal gradient of the elevation $\left(\frac{\partial Z}{\partial x}, \quad \frac{\partial Z}{\partial y}\right)$ (Sharpnack and Akin, 1969):

$$\alpha = \tan^{-1}\sqrt{\left(\frac{\partial Z}{\partial x}\right)^2 + \left(\frac{\partial Z}{\partial y}\right)^2} \tag{3}$$

$$\beta = \begin{cases} \frac{\pi}{2} - \tan^{-1}\left(\frac{\partial Z}{\partial y}/\frac{\partial Z}{\partial x}\right),\ if\frac{\partial Z}{\partial x} < 0 \\ \frac{3\pi}{2} - \tan^{-1}\left(\frac{\partial Z}{\partial y}/\frac{\partial Z}{\partial x}\right),\ if\frac{\partial Z}{\partial x} > 0 \\ undef,\ if\frac{\partial Z}{\partial x} = 0 and\ \&\ \frac{\partial Z}{\partial y} = 0 \\ 0,\ if\frac{\partial Z}{\partial x} = 0 and\ \&\ \frac{\partial Z}{\partial y} < 0 \\ \pi,\ if\frac{\partial Z}{\partial x} = 0 and\ \&\ \frac{\partial Z}{\partial y} > 0 \end{cases} \tag{4}$$

The items $\frac{\partial Z}{\partial x}$ and $\frac{\partial Z}{\partial x}$ can be calculated with the SRTM DEM data with the horizontal resolution of ~90 m by equation (5):

$$\begin{cases} \frac{\partial Z}{\partial x} = \frac{(Z_{m+1,n+1} - Z_{m-1,n+1}) + (Z_{m+1,n} - Z_{m-1,n}) + (Z_{m+1,n-1} - Z_{m-1,n-1})}{6\Delta x} \\ \frac{\partial Z}{\partial y} = \frac{(Z_{m+1,n+1} - Z_{m+1,n-1}) + (Z_{m,n+1} - Z_{m,n-1}) + (Z_{m-1,n+1} - Z_{m-1,n-1})}{6\Delta y} \end{cases} \tag{5}$$

Where $\Delta x$ and $\Delta y$ are the zonal and meridional grid distance of the SRTM DEM data. $m$ ($n$) represents the grid number along the west-east (south-north) directions, respectively.

We have developed a 3DSTLRE scheme (Gu *et al* 2024a) that utilizes the grid-scale terrain correction factor to correct the SDLR fluxes simulated by the numerical models adopting the plane-parallel approach:

$$L_{t,g\downarrow} = L_{p,g\downarrow}{\cdot}C_1 + L_{p,g\uparrow}{\cdot}C_2 \tag{6}$$

$$C_1 = (\sum_{i=1}^{i=N} SVF_i{\cdot}\sec\alpha_i)/(\sum_{i=1}^{i=N}\sec\alpha_i) \tag{7}$$

$$C_2 = \left[\sum_{i=1}^{i=N}(1 - SVF_i) \bullet \sec\alpha_i\right]/(\sum_{i=1}^{i=N}\sec\alpha_i) \tag{8}$$

Where $L_{t,g\downarrow}$ is the grid-scale SDLR corrected by the 3DSTLRE scheme. $L_{p,g\downarrow}$ and $L_{p,g\uparrow}$ are the grid-scale SDLR and SULR fluxes simulated by the numerical models adopting the plane-parallel radiative transfer scheme. The terrain correction factors $C_1$ and $C_2$ represent the grid-scale sky view factor and terrain view factor, respectively, which take into account the surface area variation of rugged terrains. Sum of $C_1$and $C_2$is 1.0. Smaller $C_1$ and larger $C_2$ indicate that the grid has more complex sub-grid terrain, resulting in stronger 3DSTLRE. More details can be found in Gu *et al* (2024a). The difference between the SDLR with and without the 3DSTLRE correction is

$$(L_{t,g\downarrow} - L_{p,g\downarrow}) = L_{p,g\downarrow}{\cdot}C_1 + L_{p,g\uparrow}{\cdot}C_2 - L_{p,g\downarrow}. \tag{9}$$

Taking $C_2 = 1 - C_1$ into equation (9), equation (9) can be rewritten as

$$(L_{t,g\downarrow} - L_{p,g\downarrow}) = (L_{p,g\uparrow} - L_{p,g\downarrow}){\cdot}C_2 \tag{10}$$

$C_2$is static data and doesn't change over time. The item ($L_{p,g\uparrow} - L_{p,g\downarrow}$) is the surface outgoing net longwave radiation calculated by the plane-parallel radiative transfer module of the numerical model.

### 2.3. Offline Correction of 3DSTLRE

As shown in figure 1(d), the monthly SDLR fluxes are corrected at their native grid according to equations (6)–(8). The monthly SDLR fluxes corrected by the 3DSTLRE are then remapped onto the grids with a horizontal resolution of 1.0° using the first-order conservative remapping method (Jones 1999). The multi model ensemble (MME) mean SDLR fluxes without and with the 3DSTLRE correction are referred as the MME_PP data and the MME_TOP data, respectively. The abbreviations 'PP' and 'TOP' stand for plane-parallel and topography slope, respectively. The hourly SDLR fluxes provided by the TPDC are averaged to monthly SDLR. The monthly SDLR fluxes from the CLARA-A2, the TPDC, and the CERES are remapped to the grids with a horizontal resolution of 1.0°. The monthly SDLR fluxes averaged from the CLARA-A2, the TPDC, and the CERES with a horizontal resolution of 1.0° are referred to as the observational (OBS) data and considered the 'true value'. The 3DSTLRE correction factors are determined solely by the sub-grid terrain and are not influenced by time. The absence of diurnal variation in the longwave radiation emitted by the terrain and the atmosphere does not affect the accuracy of the 3DSTLRE correction.

### 2.4. Metrics

The relative root mean square error (RRMSE), relative error (RE), and absolute relative error (ARE) are used to evaluate the performance of the simulated SDLR fluxes and calculated by equations (11)–(13):

$$RRMSE = \frac{\sqrt{\sum_{i=1}^{n}(S_i - O_i)^2}}{\sum_{i=1}^{n} O_i} \times 100\% \tag{11}$$

$$RE = \frac{S - O}{O} \times 100\% \tag{12}$$

$$ARE = \left| \frac{S - O}{O} \times 100\% \right| \tag{13}$$

Where $O$ and $S$ represent the observation and the model simulation, respectively, $n$ is the sample size. The correction and evaluation are conducted over the land of East Asia (65°E ~ 145°E, 17°N ~ 59°N, figures 1(a) and (e)).

## 3. Results

As shown in Figures 2(a1)–(e2), the SDLR simulations in the MME_PP data can reproduce the spatial distributions of the annual and seasonal SDLR. Due to the absence of 3DSTLRE, the annual and seasonal SDLR in the MME_PP data show more pronounced underestimation over the rugged areas compared to those over flat surfaces (Figures 2(a4)–(e4)). The underestimations of the SDLR without correction in the MME_PP data can exceed 18 W·m$^{-2}$, with the most significant underestimations located over the edge of the Tibetan Plateau, particularly along the western edge. Compared to the MME_PP data without correction, the SDLR fluxes in the MME_TOP data with the offline correction of 3DSTLRE can be increased by 3~18 W·m$^{-2}$ in each season (figures 2(a5)–(e5)), indicating that the correction helps to mitigate the underestimation present in the uncorrected SDLR. The increase in SDLR resulting from the offline correction of 3DSTLRE is due to the fact that the SDLR emitted from the surrounding terrain is usually greater than that emitted from the atmosphere (Hoch and Whiteman 2010). This leads to a higher SDLR over rugged surfaces compared to flat surfaces at the same time and in the same locations (Sicart *et al* 2006, Feldman *et al* 2022). The variations in the magnitude of increased SDLR due to the 3DSTSRE across different seasons can be attributed to the differences in surface net longwave radiation, as calculated by the plane-parallel radiative transfer module during these seasons (see equation (10)).

Figures 2(a6)–(e7) demonstrate that the offline correction can significantly reduce the RRMSE of the simulated SDLR in the MME_TOP data compared to the MME_PP data in rugged regions, especially over the Tibetan Plateau. The RRMSE of the simulated SDLR in the MME_TOP data can be reduced by 10% ~ 50% over most of the grids with the $C_1 \leqslant 0.99$ compared to those in the MME_PP data throughout the year Figures 2(a8)–(e8)). Although the East Asia has various climatic zones (see figure 5 in Kim and Bae, 2021), the effects of the 3DSTLRE are not sensitive to variations in climatic types. The effects of the 3DSTLRE primarily depend on the complexity of the terrain (figures 1(a), (e), 3(a8)–(e8)). The 3DSTLRE is most effective over the Himalayas, the Tibetan Plateau, the Tianshan Mountains, and the Hengduan Mountains. The Tibetan Plateau has significant thermal impacts on the East Asia Monsoon (Duan *et al* 2020). Therefore, the 3DSTLRE should be incorporated into numerical models. The numbers in figures 2(a1)–(e3) show the regional average values and RRMSEs of the annual and seasonal SDLR over the grids

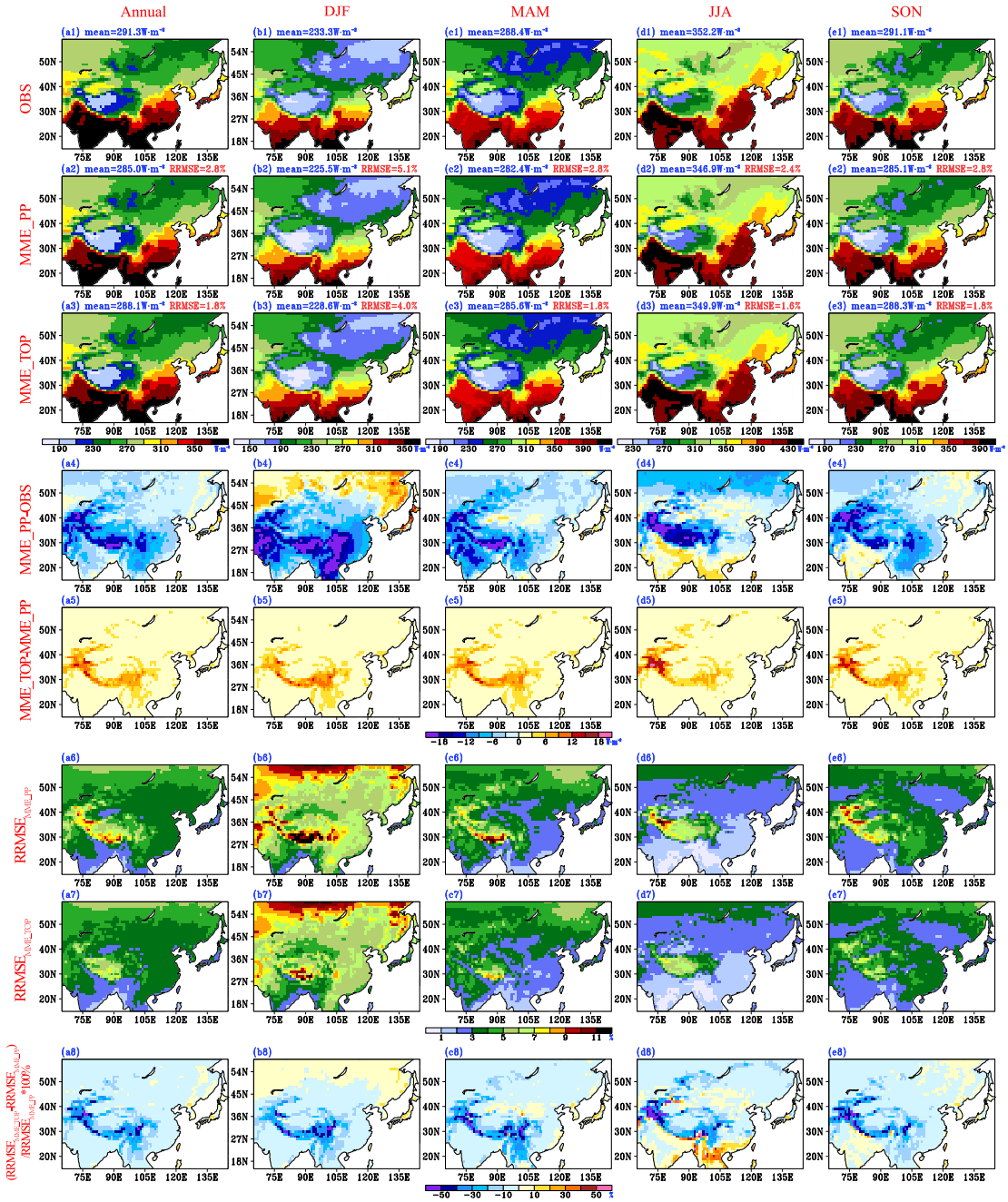


**Figure 2.** The surface downward longwave radiation (SDLR) with a horizontal resolution of 1.0° from the OBS data (a1)–(e1), the MME_PP data (a2)–(e2), and the MME_TOP data (a3)–(e3) averaged over 2001~2014. The differences of the 14-year mean SDLR fluxes between the MME_PP data and the OBS data (a4)–(e4), and between the MME_TOP data and the MME_PP data (a5)–(e5). The relative root mean square errors (RRMSE) of the SDLR from the MME_PP data (a6)–(e6) and the MME_TOP data (a7)–(e7) during 2001–2014. The relative differences of the RRMSE of the SDLR between the MME_TOP data and the MME_PP data (a8)–(e8) during 2001–2014. The blue numbers in figures (a1)–(e3) are the SDLR averaged at the grids with $C_1 \leqslant 0.99$ shown in figure 1(e). The red numbers in Figures (a2)–(e3) are the RRMSEs of the SDLR simulations during 2001–2014 at the grids with $C_1 \leqslant 0.99$ shown in figure 1(e), respectively. $C_1$ represents the grid-scale sky view factor and a smaller $C_1$ value indicates more complex sub-grid terrain.

with $C_1 \leqslant 0.99$, indicating better performance of the SDLR simulations in the MME_TOP data than in the MME_PP data.

Figures 3(a)–(e) shows the annual and seasonal RRMSEs of the SDLR simulations from the MME_PP and MME_TOP data during 2001–2014. The annual and seasonal RRMSE of SDLR in the MME_PP data increases with the 3DSTLRE correction factor $C_1$ decreasing. In other words, RRMSE increases with the sub-grid terrain complexity (figures 3(a)–(e), 1(a), and (e)). With the offline correction of 3DSTLRE, the RRMSE of the SDLR in the MME_TOP data is evidently reduced over the rugged terrain compared to that in the MME_PP data (figures 3(a)–(e), 1(a), and (e)). Throughout the year, the RRMSE of the SDLR over the mountainous areas ($C_1 \leqslant 0.99$) in the MME_TOP data is almost equal to that over the plain surfaces ($0.99 < C_1 \leqslant 1$), indicating that the

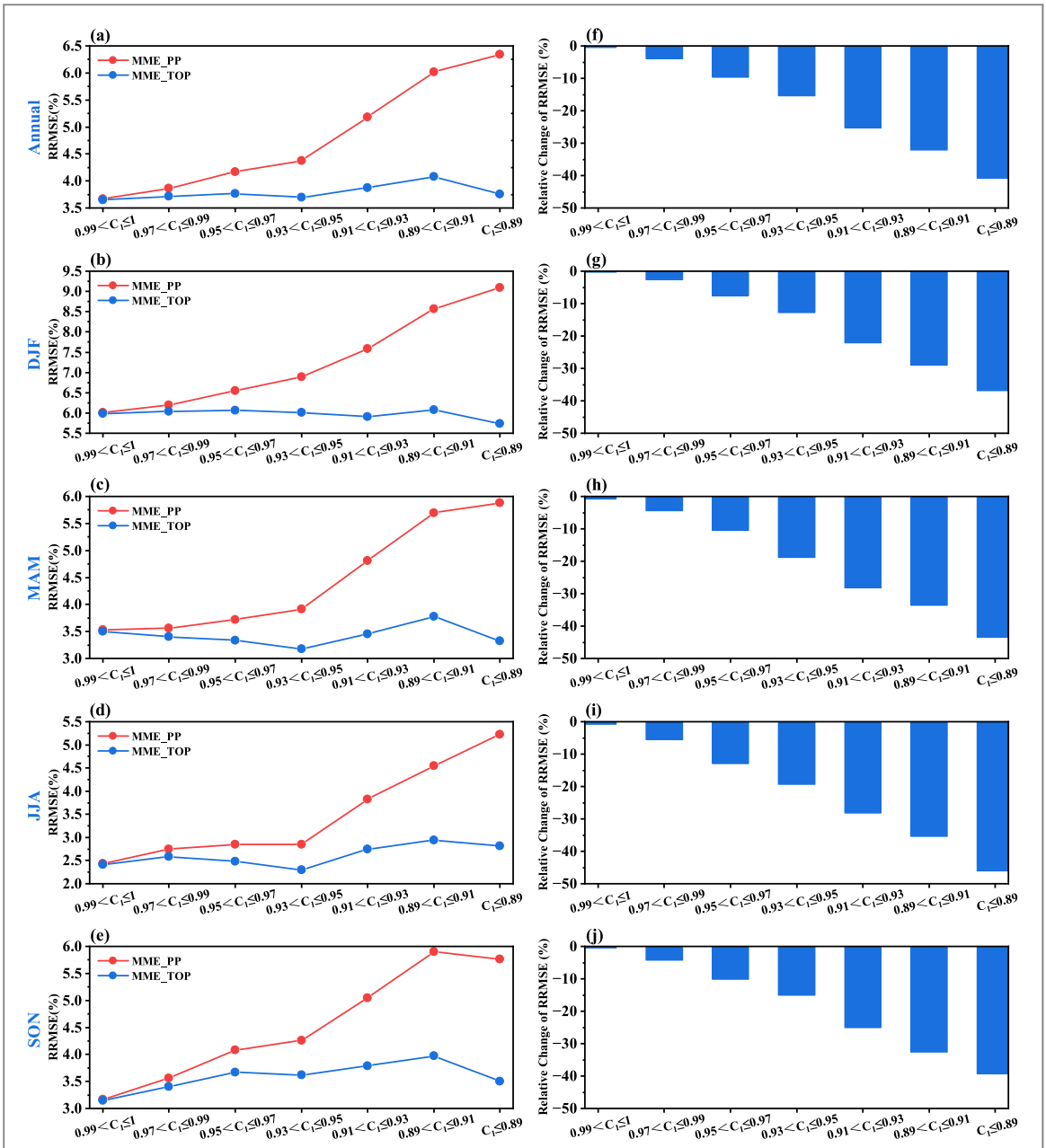


**Figure 3.** The annual and seasonal relative root mean square errors (RRMSE) of the SDLR simulations from the MME_PP and MME_TOP data during 2001–2014 (a)–(e), and the annual and seasonal relative changes of the relative root mean square errors of the SDLR simulations with the 3DSTLRE offline correction during 2001–2014 compared to those without the 3DSTSRE offline correction at the grids with different grid-scale $C_1$ shown in figure 1(e). $C_1$ represents the grid-scale sky view factor and a smaller $C_1$ value indicates more complex sub-grid terrain.

offline correction can successfully remove the biases due to neglecting the 3DSTLRE in the CMIP6 HighResMIP models. The output from global climate models (GCMs) can serve as input data for the offline operation of land surface models or hydrological models. By employing the method introduced in this study and in Gu *et al* (2024b), we can reduce the uncertainty in the simulated SDLR and surface downward solar radiation in rugged regions to levels comparable to those found in flat terrain. This enhancement will facilitate more accurate predictions of processes such as glacial dynamics, runoff, and vegetation growth in complex landscapes.

The relative reduction in the RRMSE of the SDLR between the MME_TOP data and the MME_PP data increases with the sub-grid terrain complexity (figures 3(f)–(j)). Over the grids with the most complex sub-grid terrains ($C_1 \leqslant 0.89$), the RRMSE of the annual, winter, spring, summer, and autumn SDLR in the MME_TOP data can be decreased by 40.9%, 37.0%, 43.4%, 46.0%, and 39.3% due to the offline correction of 3DSTLRE, respectively.

The probability density function (PDF, figures 4(a)–(e)) of the absolute relative error of the monthly SDLR simulations shows that the 3DSTLRE offline correction clearly decreases the probability of relatively higher absolute relative errors and increases the probability of relatively lower absolute relative errors in different

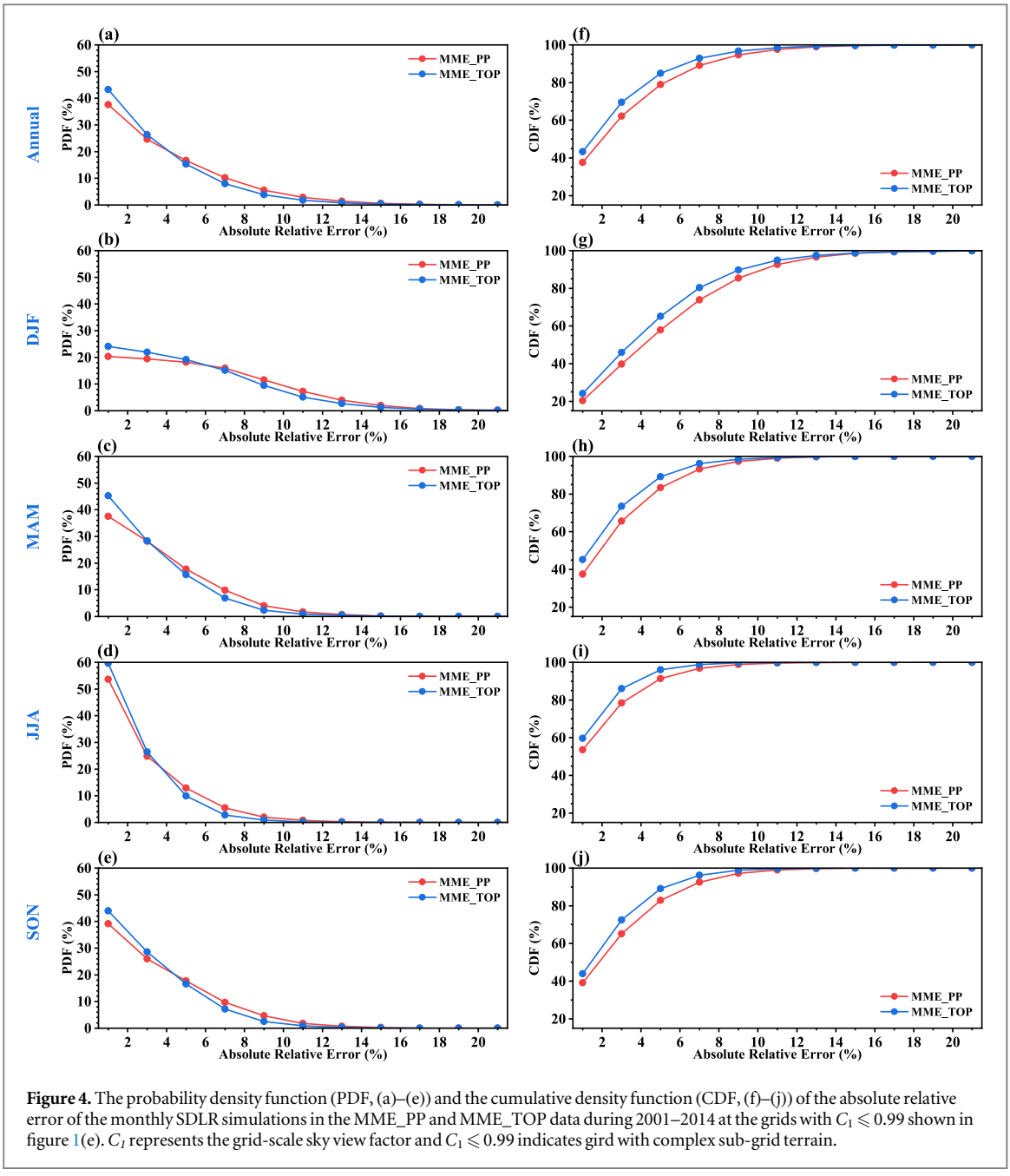


**Figure 4.** The probability density function (PDF, (a)–(e)) and the cumulative density function (CDF, (f)–(j)) of the absolute relative error of the monthly SDLR simulations in the MME_PP and MME_TOP data during 2001–2014 at the grids with $C_1 \leqslant 0.99$ shown in figure 1(e). $C_1$ represents the grid-scale sky view factor and $C_1 \leqslant 0.99$ indicates gird with complex sub-grid terrain.

seasons. The cumulative density functions (CDF, figures 4(f)–(j)) of the absolute relative error (ARE) of the monthly SDLR simulations in the MME_TOP and MME_PP data also demonstrate that the offline correction of 3DSTLRE can significantly reduce the absolute relative errors of the simulated SDLR over the rugged area. In the MME_TOP data, there are approximately 6.0%, 7.3%, 5.8%, 4.7%, and 6.2% more grids with the ARE of simulated annual, winter, spring, summer, and autumn SDLR less than 5%, respectively, compared to those in the MME_PP data.

## 4. Conclusion and discussion

The three-dimensional structure of sub-grid terrain significantly regulates the SDLR by obstructing the SDLR from the atmosphere and emitting the SDLR from the surrounding terrains to the target point. These effects are referred to as the 3DSTLRE. However, the CMIP6 HighResMIP6 models do not account for the 3DSTLRE at all. The absence of 3DSTLRE can introduce additional uncertainty and relatively larger biases in the SDLR simulations over the grids with complex sub-grid terrain compared to the grids with flat sub-grid terrain. The SDLR simulated by the CMIP6 HighResMIP6 models is widely utilized in climate research and can be served as the forcing data for land surface models, glacier models, and hydrological models. There is a need to assess the

additional uncertainty and biases in the SDLR simulated by the CMIP6 HighResMIP models and develop a method to mitigate this additional uncertainty and model bias.

In this study, the 3DSTLRE scheme (Gu *et al* 2024a) is adopted to rectify the monthly CMIP6 HighResMIP SDLR simulations and then SDLR simulations with and without the offline correction are evaluated. Results show that the multi-model ensemble mean SDLR simulations of the CMIP6 HighResMIP are clearly underestimated over the regions with complex terrain, and the underestimations increase with the sub-grid terrain complexity. The offline correction of 3DSTLRE can significantly reduce the biases of the CMIP6 HighResMIP SDLR simulations, and the improvements increases with the sub-grid terrain complexity. At the grids with the most complex sub-grid terrain ($C_1 \leqslant 0.89$), the RRMSE of the annual, winter, spring, summer, and autumn SDLR simulations of the CMIP6 HighResMIP can be decreased by 40.9%, 37.0%, 43.4%, 46.0%, and 39.3% due to the 3DSTLRE offline correction, respectively. The RRMSE of the corrected SDLR simulations in the rugged areas is almost equal to that in the plane areas, suggesting that the biases of the SDLR simulated by the CMIP6 HighResMIP models without the 3DSTLRE can be efficiently eliminated by the offline correction of 3DSTLRE.

The results of this study indicate that it is a great necessity to consider the 3DSTLRE to improve the SDLR simulations. The 3DSTLRE-corrected SDLR from the CMIP6 HighResMIP can be better utilized in climate research. However, this study has the following shortcomings: (1) due to limitations in workload and computational resources, we were unable to apply 3DSTLRE to the 11 CMIP6 HighResMIP models for online simulation of SDLR. Instead, we performed offline corrections on the SDLR outputs of these 11 models. Therefore, the feedback of the land-atmosphere processes to the 3DSTLRE is completely neglected in this study. Previous studies indicate that the improved simulation of SDLR can enhance the modeling of land surface processes, including snow cover and soil hydrothermal states (Luo *et al* 2023, Pomeroy *et al* 2009). We guess that the simulated atmosphere would then be adjusted in response to the enhanced simulation of these land surface processes, potentially leading to further improvements in the simulation of SDLR. It is essential to conduct online sensitivity numerical experiments in regions with diverse climate types and varying terrain complexities to test this hypothesis. (2) Due to the lack of diurnal observations, the performance of the diurnal variation of the SDLR with or without the 3DSTLRE correction was not evaluated in this study. This study missed the opportunity to observe the maximum impacts of 3DSTLRE on the simulated SDLR within the day. Therefore, it is essential to gain a deeper understanding of the diurnal variation of 3DSTLRE in the future. We will discuss these topics when we report the impacts of the 3DSTLRE parameterization on the performance of Regional Climate Model Version 4 (RegCM4) in the near future.

## Acknowledgments

This study is supported by the National Natural Science Foundation of China under Grant 42375157, the National Key Research and Development Program of China (2022YFC3080500), the National Key R&D Program of China under Grant 2022YFC3080500, the CAS 'Light of West China' Program (E129030101), Open Research Fund Program of Plateau Atmosphere and Environment Key Laboratory of Sichuan Province (PAEKL-2023-K01), and the Beijige Open Research Fund under Grant BJG202403. We appreciate the High Performance Computing Center of Nanjing University and the National Key Scientific and Technological Infrastructure project 'Earth System Numerical Simulation Facility' (EarthLab) for providing us the computing resource. We are grateful to ESGF, CIAT, NASA, EUMETSAT, and TPDC for allowing us to use their datasets. We appreciate Dr. Weidan Zhou's assistance with computational resources. We extend our heartfelt gratitude to the editor and the two anonymous reviewers for their valuable and insightful feedback, which has greatly contributed to improving the quality of our manuscript.

## Data availability statement

All data that support the findings of this study are included within the article (and any supplementary files).

## ORCID iDs

Chunlei Gu https://orcid.org/0000-0001-7019-2392
Anning Huang https://orcid.org/0000-0001-9872-440X
Xin Li https://orcid.org/0000-0002-8539-6504
Yang Wu https://orcid.org/0000-0002-3477-7171

## References


An B *et al* 2022 CAS FGOALS-f3-H dataset for the high-resolution model intercomparison project (HighResMIP) tier 2 *Adv. Atmos. Sci.* **39** 1873–84

Arnold N S, Rees W G, Hodson A J and Kohler J 2006 Topographic controls on the surface energy balance of a high Arctic valley glacier *Journal of Geophysical Research: Earth Surface* **111** 2781–9

Arthur R S, Lundquist K A, Mirocha J D and Chow F K 2018 Topographic effects on radiation in the WRF model with the immersed boundary method: implementation, validation, and application to complex terrain *Mon. Weather Rev.* **146** 3277–92

Aubry-Wake C, ZÉPhir D, Baraer M, McKenzie J M and Mark B G 2018 Importance of longwave emissions from adjacent terrain on patterns of tropical glacier melt and recession *Journal of Glaciology* **64** 49–60

Cai S, Huang A, Zhu K, Guo W, Wu Y and Gu C 2023 The forecast skill of the summer precipitation over tibetan plateau improved by the adoption of a 3D sub-grid terrain solar radiative effect scheme in a convection-permitting model *Journal of Geophysical Research: Atmospheres* **128** e2022JD038105

Chang P *et al* 2020 An unprecedented set of high-resolution earth system simulations for understanding multiscale interactions in climate variability and change *Journal of Advances in Modeling Earth Systems* **12** e2020MS002298

Chen G, Zhang X and Fu Y 2022 Diurnal variation in clouds and radiative budgets over the tibetan plateau during summer using CERES data *Journal of Geophysical Research: Atmospheres* **127** e2021JD036329

Chen Y, Hall A and Liou K N 2006 Application of three-dimensional solar radiative transfer to mountains *Journal of Geophysical Research Atmospheres* **111** 1–13

Cole R J 1979 The longwave radiation incident upon inclined surfaces *Sol. Energy* **22** 459–62

Dirksen M, Ronda R J, Theeuwes N E and Pagani G A 2019 Sky view factor calculations and its application in urban heat island studies *Urban Climate* **30** 100498

Doelling D R, Sun M, Le T N, Nordeen M L and Mlynczak P E 2016 Advances in geostationary-derived longwave fluxes for the ceres synoptic (syn1deg) product *Journal of Atmospheric & Oceanic Technology* **33** 160118113337004

Dozier J and Outcalt S 1979 An approach toward energy balance simulation over rugged terrain *Geographical Analysis* **11** 65–85

Dozier J and Frew J 1990 Rapid calculation of terrain parameters for radiation modeling from digital elevation data *IEEE Trans. Geosci. Remote Sens.* **28** 963–9

Duan A, Hu D, Hu W and Zhang P 2020 Precursor effect of the tibetan plateau heating anomaly on the seasonal march of the East Asian summer monsoon precipitation *Journal of Geophysical Research: Atmospheres* **125** e2020JD032948

Duguay C R 1993 Modelling the radiation budget of alpine snowfields with remotely sensed data: model formulation and validation *Ann. Glaciol.* **17** 288–94

EC-Earth Consortium 2018 EC-Earth-Consortium EC-Earth3P-HR model output prepared for CMIP6 HighResMIP hist-1950 [Datasets], Retrieved from:

Essery R and Marks D 2007 Scaling and parametrization of clear-sky solar radiation over complex topography *Journal of Geophysical Research: Atmospheres* **112** D10122

Fan X, Gu Y, Liou K-N, Lee W-L, Zhao B, Chen H and Lu D 2019 Modeling study of the impact of complex terrain on the surface energy and hydrology over the Tibetan Plateau *Clim. Dyn.* **53** 6919–32

Feldman D R, Worden M, Falco N, Dennedy-Frank P J, Chen J, Dafflon B and Wainwright H 2022 Three-dimensional surface downwelling longwave radiation clear-sky effects in the upper colorado river basin *Geophys. Res. Lett.* **49** e2021GL094605

Feng C, Zhang X, Xu J, Yang S, Guan S, Jia K and Yao Y 2023 Comprehensive assessment of global atmospheric downward longwave radiation in the state-of-the-art reanalysis using satellite and flux tower observations *Clim. Dyn.* **60** 1495–521

Feng L and Zhang Y 2007 Impacts of the thermal effects of sub-grid orography on the heavy rainfall events along the Yangtze River Valley in 1991 *Adv. Atmos. Sci.* **24** 881–92

Gratton D J, Howarth P J and Marceau D J 1993 Using Landsat-5 thematic mapper and digital elevation data to determine the net radiation field of a Mountain Glacier *Remote Sens. Environ.* **43** 315–31

Gu C *et al* 2022 The wet bias of RegCM4 over tibet plateau in summer reduced by adopting the 3D sub-grid terrain solar radiative effect parameterization scheme *Journal of Geophysical Research: Atmospheres* **127** e2022JD037434

Gu C, Huang A, Wu Y, Yang B, Mu X, Zhang X and Cai S 2020 Effects of subgrid terrain radiative forcing on the ability of RegCM4.1 in the simulation of summer precipitation over China *Journal of Geophysical Research: Atmospheres* **125**

Gu C, Huang A, Li X, Yang B and Wu Y 2024a Construction of a clear-sky three dimensional sub-grid terrain long-wave radiative effect parameterization scheme under isotropic assumption *Journal of Geophysical Research: Atmospheres* **129** e2023JD039383

Gu C, Huang A, Li X and Wu Y 2024b Offline correction of CMIP6 HighResMIP simulated surface solar irradiance with 3D sub-grid terrain radiative effects *Geophys. Res. Lett.* **51** e2023GL107737

Gu Y, Liou K N, Lee W L and Leung L R 2012 Simulating 3D radiative transfer effects over the Sierra Nevada Mountains using WRF *Atmos. Chem. Phys.* **12** 9965–76

Gui S, Liang S and Li L 2010 Evaluation of satellite-estimated surface longwave radiation using ground-based observations *Journal of Geophysical Research: Atmospheres* **115** D18214

Gutjahr O *et al* 2019 Max planck institute earth system model (MPI-ESM1.2) for the high-resolution model intercomparison project (HighResMIP) *Geosci. Model Dev.* **12** 3241–81

Haarsma R *et al* 2020 HighResMIP versions of EC-Earth: EC-Earth3P and EC-Earth3P-HR—description, model computational performance and basic validation *Geosci. Model Dev.* **13** 3507–27

Haarsma R J *et al* 2016 High resolution model intercomparison project (HighResMIP v1.0) for CMIP6 *Geosci. Model Dev.* **9** 4185–208

Hao D, Bisht G, Gu Y, Lee W-L, Liou K-N and Leung L R 2021 A parameterization of sub-grid topographical effects on solar radiation in the E3SM Land Model (version 1.0): implementation and evaluation over the Tibetan Plateau *Geosci. Model Dev.* **14** 6273–89

Hauge G and Hole L R 2003 Implementation of slope irradiance in Mesoscale Model version 5 and its effect on temperature and wind fields during the breakup of a temperature inversion *Journal of Geophysical Research: Atmospheres* **108** 4058

He S, Smirnova T G and Benjamin S G 2019 A scale-aware parameterization for estimating subgrid variability of downward solar radiation using high-resolution digital elevation model data *Journal of Geophysical Research: Atmospheres* **124** 13680–92

Heavens N G 2021 Downscaling CESM2 in CLM5 to hindcast preindustrial equilibrium altitudes for tropical mountain glaciers *Geophys. Res. Lett.* **48** e2021GL094071

Hoch S W and Whiteman C D 2010 Topographic effects on the surface radiation balance in and around arizona's meteor crater *Journal of Applied Meteorology & Climatology* **49** 1114–28

Huang A *et al* 2022 Development of a clear-sky 3D sub-grid terrain solar radiative effect parameterization scheme based on the mountain radiation theory *Journal of Geophysical Research: Atmospheres* **127** e2022JD036449
Huang J, Zhou X, Wu G, Xu X, Zhao Q, Liu Y and Qie K 2023 Global climate impacts of land-surface and atmospheric processes over the tibetan plateau *Rev. Geophys.* **61** e2022RG000771
Hurrel J *et al* 2020 NCAR CESM1-CAM5-SE-HR model output prepared for CMIP6 HighResMIP hist-1950 [datasets] Retrieved from: https://highresmip.org/data/
Jarvis A, Reuter H I, Nelson A and Guevara E 2008 The Shuttle Radar Topography Mission (SRTM) 90 m Digital Elevation Database v4.1 [Dataset]. International Centre for Tropical Agriculture (CIAT) Retrieved from: https://developers.google.com/earth-engine/datasets/catalog/CGIAR_SRTM90_V4
Jiao Z H, Ren H, Mu X, Zhao J, Wang T and Dong J 2019 Evaluation of four sky view factor algorithms using digital surface and elevation model data *Earth and Space Science* **6** 222–37
Jie W *et al* 2020 BCC BCC-CSM2HR model output prepared for CMIP6 HighResMIP hist-1950 [Datasets] Retrieved from:
Jones P W 1999 First- and second-order conservative remapping schemes for grids in spherical coordinates *Mon. Weather Rev.* **127** 2204–10
Juszak I and Pellicciotti F 2013 A comparison of parameterizations of incoming longwave radiation over melting glaciers: model robustness and seasonal variability *J. Geophys. Res. Atmos.* **118** 3066–84
Karlsson K G *et al* 2017 CLARA-A2: the second edition of the CM SAF cloud and radiation data record from 34 years of global AVHRR data *Atmos. Chem. Phys.* **17** 5809–28
Karlsson K-G *et al* 2020 CLARA-A2.1: CM SAF cLoud, Albedo and surface RAdiation data set from AVHRR data - Edition 2.1 [Dataset] *Satellite Application Facility on Climate Monitoring* Retrieved from
Kim J-B and Bae D-H 2021 The impacts of global warming on climate zone changes over asia based on CMIP6 projections *Earth and Space Science* **8** e2021EA001701
Lai Y J, Chou M D and Lin P H 2010 Parameterization of topographic effect on surface solar radiation *Journal of Geophysical Research: Atmospheres* **115** D01104
Lee W-L, Liou K N and Hall A 2011 Parameterization of solar fluxes over mountain surfaces for application to climate models *Journal of Geophysical Research: Atmospheres* **116** D01101
Lee W-L *et al* 2019 Relating precipitating ice radiative effects to surface energy balance and temperature biases over the Tibetan Plateau in winter *Journal of Geophysical Research: Atmospheres* **124** 12455–67
Liou K N, Lee W-L and Hall A 2007 Radiative transfer in mountains: application to the Tibetan Plateau *Geophys. Res. Lett.* **34** L23809
Liu S, Liu Z, Duan Q and Huang B 2023 The performance of CMIP6 models in simulating surface energy fluxes over global continents *Clim. Dyn.* **61** 579–94
Luo J, Huang A, Lyu S, Lin Z, Gu C, Li Z and Liu W 2023 Improved performance of CLM5.0 model in frozen soil simulation over tibetan plateau by implementing the vegetation emissivity and gravel hydrothermal schemes *Journal of Geophysical Research: Atmospheres* **128** e2022JD038021
Manners J, Vosper S B and Roberts N 2012 Radiative transfer over resolved topographic features for high-resolution weather prediction *Q. J. R. Meteorolog. Soc.* **138** 720–33
Matzinger N, Andretta M, Gorsel E V, Vogt R, Ohmura A and Rotach M W 2003 Surface radiation budget in an alpine valley *Q. J. R. Meteorolog. Soc.* **129** 877–95
Müller M D and Scherer D 2005 A grid- and subgrid-scale radiation parameterization of topographic effects for mesoscale weather forecast models *Mon. Weather Rev.* **133** 1431–42
Naud C M, Miller J R and Landry C 2012 Using satellites to investigate the sensitivity of longwave downward radiation to water vapor at high elevations *Journal of Geophysical Research: Atmospheres* **117** D05101
Olyphant G A 1986 Longwave radiation in mountainous areas and its influence on the energy balance of alpine snowfields *Water Resour. Res.* **22** 62–6
Pomeroy J W, Marks D, Link T, Ellis C, Hardy J, Rowlands A and Granger R 2009 The impact of coniferous forest temperature on incoming longwave radiation to melting snow *Hydrol. Processes* **23** 2513–25
Priestley M D K and Catto J L 2022 Improved representation of extratropical cyclone structure in HighResMIP Models *Geophys. Res. Lett.* **49** e2021GL096708
Ren Z, Su F, Xu B, Xie Y and Kan B 2018 A coupled glacier-hydrology model and its application in eastern pamir *Journal of Geophysical Research: Atmospheres* **123** 13,692–613
Roberts C D, Senan R, Molteni F, Boussetta S and Keeley S 2017 ECMWF ECMWF-IFS-HR model output prepared for CMIP6 HighResMIP hist-1950 [Datesets], Retrieved from
Roberts C D, Senan R, Molteni F, Boussetta S, Mayer M and Keeley S P E 2018 Climate model configurations of the ECMWF Integrated Forecasting System (ECMWF-IFS cycle 43r1) for HighResMIP *Geosci. Model Dev.* **11** 3681–712
Roberts M 2021 MOHC HadGEM3-GC31-HH model output prepared for CMIP6 HighResMIP hist-1950 [Datasets], Retrieved from:
Roberts M J *et al* 2019 Description of the resolution hierarchy of the global coupled HadGEM3-GC3.1 model as used in CMIP6 HighResMIP experiments *Geosci. Model Dev.* **12** 4999–5028
Roberts M J *et al* 2020 Projected future changes in tropical cyclones using the CMIP6 HighResMIP multimodel ensemble *Geophys. Res. Lett.* **47** e2020GL088662
Robledano A, Picard G, Arnaud L, Larue F and Ollivier I 2022 Modelling surface temperature and radiation budget of snow-covered complex terrain *The Cryosphere* **16** 559–79
Ruiz-Arias J A, Pozo-Vázquez D, Lara-Fanego V, Santos-Alamillos F J and Tovar-Pescador J 2011 A high-resolution topographic correction method for clear-sky solar irradiance derived with a numerical weather prediction model *Journal of Applied Meteorology & Climatology* **50** 2460–72
Saint-Martin D *et al* 2021 Tracking changes in climate sensitivity in CNRM climate models *Journal of Advances in Modeling Earth Systems* **13** e2020MS002190
Scoccimarro E, Bellucci A and Peano D 2018 CMCC CMCC-CM2-VHR4 model output prepared for CMIP6 HighResMIP hist-1950 [Datasets], Retrieved from:
Scoccimarro E, Peano D, Gualdi S, Bellucci A, Lovato T, Fogli P G and Navarra A 2022 Extreme events representation in CMCC-CM2 standard and high-resolution general circulation models *Geosci. Model Dev.* **15** 1841–54
Senese A, Manara V, Maugeri M and Diolaiuti G A 2020 Comparing measured incoming shortwave and longwave radiation on a glacier surface with estimated records from satellite and off-glacier observations: a case study for the Forni Glacier, Italy *Remote Sensing* **12** 3719

Shakespeare C J and Roderick M L 2022 Diagnosing instantaneous forcing and feedbacks of downwelling longwave radiation at the surface: a simple methodology and its application to CMIP5 models *J. Clim.* **35** 3785–801
Shang H, Letu H, Xu R, Wei L, Wu L, Shao J and Chen L 2024 A hybrid cloud detection and cloud phase classification algorithm using classic threshold-based tests and extra randomized tree model *Remote Sens. Environ.* **302** 113957
Sharpnack D A and Akin G 1969 An algorithm for computing slope and aspect from elevations *Photogrammetric Engineering* **35** 247–8
Shi J, Tian Z, Lang X and Jiang D 2024 Projected changes in the interannual variability of surface air temperature using CMIP6 simulations *Clim. Dyn.* **62** 431–46
Sicart J E, Pomeroy J W, Essery R L H and Bewley D 2006 Incoming longwave radiation to melting snow: observations, sensitivity and estimation in Northern environments *Hydrol. Processes* **20** 3697–708
Stephens G L, Wild M, Stackhouse P W, L'Ecuyer T, Kato S and Henderson D S 2012 The global character of the flux of downward longwave radiation *J. Clim.* **25** 2329–40
Sugita M and Brutsaert W 1993 Cloud effect in the estimation of instantaneous downward longwave radiation *Water Resour. Res.* **29** 599–605
Tana G, Ri X, Shi C, Ma R, Letu H, Xu J and Shi J 2023 Retrieval of cloud microphysical properties from Himawari-8/AHI infrared channels and its application in surface shortwave downward radiation estimation in the sun glint region *Remote Sens. Environ.* **290** 113548
Tao J and Barros A P 2018 Multi-year atmospheric forcing datasets for hydrologic modeling in regions of complex terrain—methodology and evaluation over the integrated precipitation and hydrology experiment 2014 domain *J. Hydrol.* **567** 824–42
Van Beusekom A E *et al* 2022 Hydrologic model sensitivity to temporal aggregation of meteorological forcing data: a case study for the contiguous United States *Journal of Hydrometeorology* **23** 167–83
Vargas Zeppetello L R, Donohoe A and Battisti D S 2019 Does surface temperature respond to or determine downwelling longwave radiation? *Geophys. Res. Lett.* **46** 2781–9
Viúdez-Mora A, Costa-Surós M, Calbó J and González J A 2015 Modeling atmospheric longwave radiation at the surface during overcast skies: The role of cloud base height *Journal of Geophysical Research: Atmospheres* **120** 199–214
Voldoire A 2019 CNRM-CERFACS CNRM-CM6-1-HR model output prepared for CMIP6 HighResMIP hist-1950 [Datasets], retrieved from:
Volodin E *et al* 2019 INM INM-CM5-H model output prepared for CMIP6 HighResMIP hist-1950 [Datasets], Retrieved from:
Volodin E *et al* 2017 Simulation of the present-day climate with the climate model INMCM5 *Clim. Dyn.* **49** 3715–34
von Storch J-S *et al* 2018 MPI-M MPI-ESM1.2-XR model output prepared for CMIP6 HighResMIP hist-1950 [Datasets], Retrieved from:
Wan Z, Wang W, Lyu H, Qiu P, Li Y and Lu Y 2022 Comparison between CMIP6 and CMIP5 models in simulating historical spatiotemporal variations in radiation budgets at the top of atmosphere and the surface *Climate Change Research* **18** 468–81
Wang G, Wang T and Xue H 2021 Validation and comparison of surface shortwave and longwave radiation products over the three poles *Int. J. Appl. Earth Obs. Geoinf.* **104** 102538
Wang K and Liang S 2009 Global atmospheric downward longwave radiation over land surface under all-sky conditions from 1973 to 2008 *Journal of Geophysical Research: Atmospheres* **114** D19101
Wang L, Liu Z, Lang X and Jiang D 2023 Understanding surface air temperature cold bias over China in CMIP6 models *Journal of Geophysical Research: Atmospheres* **128** e2023JD039515
Wang Q *et al* 2022 An assessment of land energy balance over East Asia from multiple lines of evidence and the roles of the Tibet Plateau, aerosols, and clouds *Atmos. Chem. Phys.* **22** 15867–86
Wang S, Wang T, Leng W, Wang G and Letu H 2022 Toward an improved global longwave downward radiation product by fusing satellite and reanalysis data *IEEE Trans. Geosci. Remote Sens.* **60** 1–16
Wang T and Wang S 2022 Fused global land surface longwave downward radiation dataset (2016-2020, 1h/0.25°) *National Tibetan Plateau / Third Pole Environment Data Center* 4133–53
Webster C, Rutter N and Jonas T 2017 Improving representation of canopy temperatures for modeling subcanopy incoming longwave radiation to the snow surface *Journal of Geophysical Research: Atmospheres* **122** 9154–72
Whiteman C D, Allwine K J, Fritschen L J, Orgill M M and Simpson J R 1989 Deep valley radiation and surface energy budget microclimates. Part I: radiation *Journal of Applied Meteorology and Climatology* **28** 414–26
Wild M 2020 The global energy balance as represented in CMIP6 climate models *Clim. Dyn.* **55** 553–77
Wu F *et al* 2024 Understanding of CMIP6 surface temperature cold bias over the westerly and monsoon regions of the Tibetan Plateau *Clim. Dyn.*
Wu T *et al* 2021 BCC-CSM2-HR: a high-resolution version of the Beijing climate center climate system model *Geosci. Model Dev.* **14** 2977–3006
Wu Y, Wang N, Li Z, Chen A, Guo Z and Qie Y 2019 The effect of thermal radiation from surrounding terrain on glacier surface temperatures retrieved from remote sensing data: a case study from Qiyi Glacier, China *Remote Sens. Environ.* **231** 111267
Wu Z, Zhang P, Chen H and Li Y 2016 Can the Tibetan Plateau snow cover influence the interannual variations of Eurasian heat wave frequency? *Clim. Dyn.* **46** 3405–17
Xu J *et al* 2022 Assessment of surface downward longwave radiation in CMIP6 with comparison to observations and CMIP5 *Atmos. Res.* **270** 106056
Yan G, Jiao Z-H, Wang T and Mu X 2020 Modeling surface longwave radiation over high-relief terrain *Remote Sens. Environ.* **237** 111556
Yan G, Wang T, Jiao Z, Mu X, Zhao J and Chen L 2016 Topographic radiation modeling and spatial scaling of clear-sky land surface longwave radiation over rugged terrain *Remote Sens. Environ.* **172** 15–27
Yan H, Huang J, Minnis P, Wang T and Bi J 2011 Comparison of CERES surface radiation fluxes with surface observations over Loess Plateau *Remote Sens. Environ.* **115** 1489–500
Yu Y 2020 CAS FGOALS-f3-H model output prepared for CMIP6 HighResMIP hist-1950 [Datasets], Retrieved from:
Zhang G *et al* 2013 Energy and mass balance of Zhadang glacier surface, central Tibetan Plateau *Journal of Glaciology* **59** 137–48
Zhang X *et al* 2022 Influences of 3D sub-grid terrain radiative effect on the performance of CoLM over heihe river basin, Tibetan Plateau *Journal of Advances in Modeling Earth Systems* **14** e2021MS002654
Zhang Y, Huang A and Zhu X 2006 Parameterization of the thermal impacts of sub-grid orography on numerical modeling of the surface energy budget over East Asia *Theor. Appl. Climatol.* **86** 201–14
Zhao M *et al* 2018a The GFDL global atmosphere and land model AM4.0/LM4.0: 2. Model description, sensitivity studies, and tuning strategies *Journal of Advances in Modeling Earth Systems* **10** 735–69
Zhao M *et al* 2018b NOAA-GFDL GFDL-CM4C192 model output prepared for CMIP6 HighResMIP hist-1950 [Datasets], Retrieved from:
Zhu X *et al* 2018 Effects of complex terrain on net surface longwave radiation in China *Theor. Appl. Climatol.* **134** 251–64